

# Modeling X-ray emission from stellar coronae

S. G. Gregory\*, M. Jardine\*, C. Argiroffi<sup>†,\*\*</sup> and J.-F. Donati<sup>‡</sup>

\**SUPA, School of Physics and Astronomy, Univ. of St Andrews, St Andrews, KY16 9SS, UK*  
<sup>†</sup>*Dipt. di Scienze Fisiche ed Astronomiche, Sezione di Astronomia, Univ. di Palermo, Piazza del Parlamento 1, 90134 Palermo, Italy*  
<sup>\*\*</sup>*INAF - Osservatorio Astronomico di Palermo, Piazza del Parlamento 1, 90134 Palermo, Italy*  
<sup>‡</sup>*LATT - CNRS/Université de Toulouse, 14 Av. E. Belin, F-31400 Toulouse, France*

**Abstract.** By extrapolating from observationally derived surface magnetograms of low-mass stars we construct models of their coronal magnetic fields and compare the 3D field geometry with axial multipoles. AB Dor, which has a radiative core, has a very complex field, whereas V374 Peg, which is completely convective, has a simple dipolar field. We calculate global X-ray emission measures assuming that the plasma trapped along the coronal loops is in hydrostatic equilibrium and compare the differences between assuming isothermal coronae, or by considering a loop temperature profiles. Our preliminary results suggest that the non-isothermal model works well for the complex field of AB Dor, but not for the simple field of V374 Peg.

**Keywords:** Stars: coronae - Stars: activity - X-rays: stars - Stars: individual: AB Dor, V374 Peg  
**PACS:** 97.10.Ex - 97.10.Jb - 97.10.Ld - 97.10.Jg

## DETECTING AND EXTRAPOLATING STELLAR FIELDS

Using the spectropolarimetric technique known as Zeeman-Doppler imaging (ZDI) it is possible to map the medium and large scale structure of stellar magnetic topologies (see Donati et al, these proceedings). From such observationally derived surface maps of the photospheric magnetic fields of the rapidly rotating K-dwarf AB Dor [1] and the low mass M-dwarf V374 Peg [2] we extrapolate the coronal fields assuming that they are potential, or current free,  $\nabla \times \mathbf{B} = \mathbf{0}$  (Fig. 1). This condition is satisfied by writing the field in terms of a scalar flux function  $\Psi$ , with  $\mathbf{B} = -\nabla\Psi$ . As the field must also be solenoidal,  $\nabla \cdot \mathbf{B} = 0$ , then  $\Psi$  must satisfy Laplace's equation  $\nabla^2\Psi = 0$ , the solution of which is a linear combination of spherical harmonics. Thus the three components of the magnetic field vector can be determined within a defined 3D volume, and a field line tracing algorithm employed to derive the coronal magnetic field topology. The extrapolation technique is described in greater detail by [3] and [4]. The stellar parameters for AB Dor and V374 Peg are listed in Table 1.

### Comparison with axial multipoles

We compare the 3D coronal field structures obtained via field extrapolation with axial multipoles (Fig. 1). The height and width of field line loops is defined in Fig. 2. The

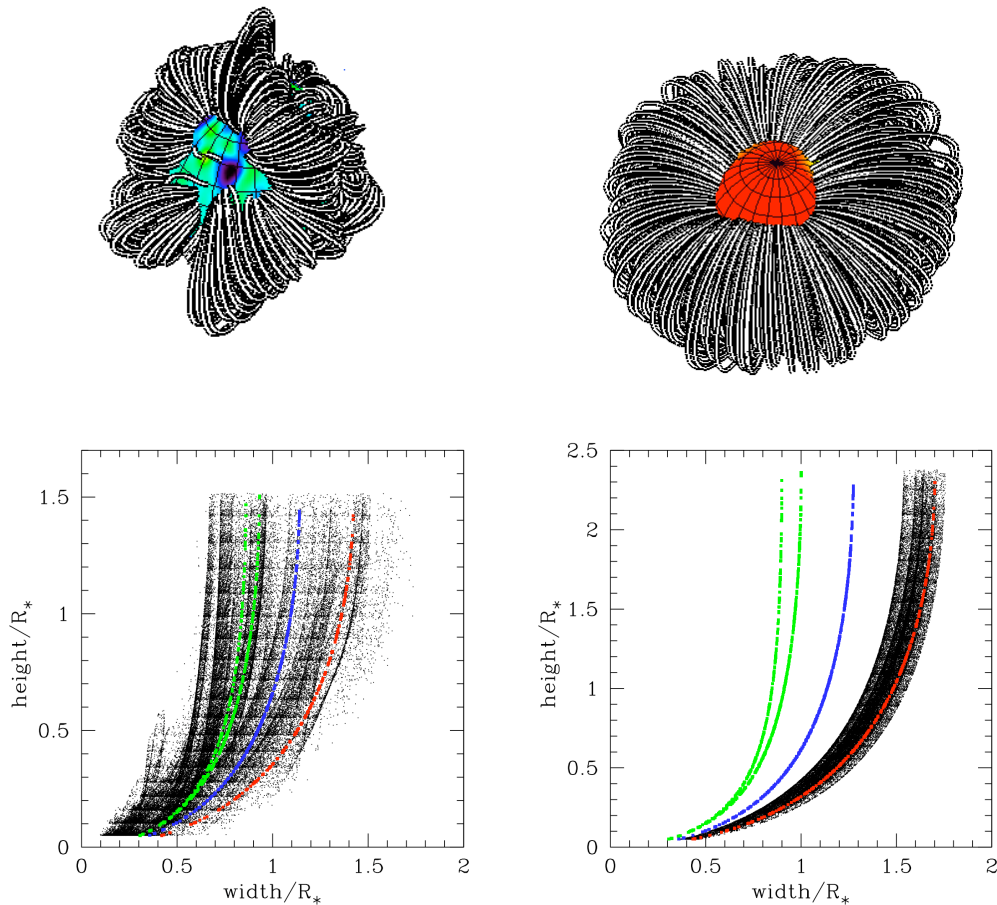


**FIGURE 1.** Field extrapolations from magnetic surface maps of AB Dor (left) and V374 Peg (right) [upper panel, not to scale]. The plots [lower panel] show field line height vs width, as defined in Fig 2, compared to axial multipoles, a dipole (red), a quadrupole (blue) and an octupole (green).

width is calculated using the Haversine formula,

$$w = 2 \sin^{-1} \left[ \sqrt{\sin^2 \left( \frac{\Delta\theta}{2} \right) + \sin \theta_1 \sin \theta_2 \sin^2 \left( \frac{\Delta\phi}{2} \right)} \right], \quad (1)$$

where  $\Delta\theta = |\theta_2 - \theta_1|$  and  $\Delta\phi = \phi_2 - \phi_1$  are the differences in co-latitudes and longitudes of the field line foot points, and where all angles are measured in radians and all distances in units of stellar radii.

V374 Peg, at only  $0.3 M_{\odot}$ , is completely convective [2] and has a large scale axisymmetric magnetic field which has been found to be remarkably stable over a timescale of at least one year [5]. Its field is almost dipolar, as evident from both the field extrapolation and from the plot of field line height vs width (Fig. 1). In contrast, AB Dor is a solar mass star with a radiative core, the star spot distribution (and therefore the magnetic

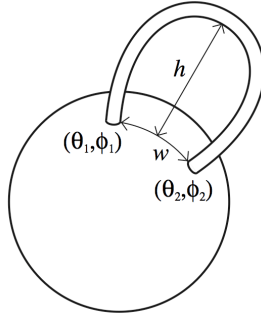


**FIGURE 2.** The width,  $w$ , of field lines is defined as the distance measured along the segment of the great circle connecting the field line foot points. It is calculated using the Haversine formula (equation 1). The height,  $h$ , is the maximum loop height above the stellar surface.

field) on which is known to vary on a timescale of at least one year [6]. The magnetic field of AB Dor is particularly complex (Fig. 1) with contributions from many high order multipole components. The difference in field complexity for both stars is likely to be a simple reflection of their different internal structures, and therefore magnetic field generation mechanisms.

## Coronal X-ray emission

We assume that the X-ray emitting plasma is trapped along the coronal loops and calculate the pressure structure along loops by integrating the equation of hydrostatic equilibrium [7]. The pressure at a point  $s$  along a loop is given by,

$$p(s) = p_0 \exp \left[ \frac{\mu m_H}{k_B} \int_0^s \frac{g_s}{T} ds \right], \quad (2)$$

where  $g_s$  is the component of the effective gravity (i.e. the component of the combined centrifugal and gravitational acceleration) along the direction of the field at  $s$ , and  $g_s = \mathbf{g} \cdot \mathbf{B} / |\mathbf{B}|$ . Assuming that the pressure and density are related via  $p = 2nk_B T$  then the global X-ray emission measure can be calculated as described by [7]. We set the coronal pressure to zero for open field lines and for loops which would be unable to contain the coronal plasma due to the gas pressure exceeding the magnetic pressure. Such regions therefore do not contribute to the X-ray emission. X-ray emitting gas is typically contained within compact magnetic regions, however some regions of the stellar surface remain dark in X-rays, giving rise to modulation of X-ray emission, especially for AB Dor.

Table 2 shows the simulated X-ray emission properties when assuming an isothermal corona (at 10MK for AB Dor and 20MK for V374 Peg). Also shown for comparison are the same quantities derived by considering a Serio-type temperature scaling law [8], where the loop temperatures depend on the pressure at the loop foot points, the length of the loop, and a (somewhat arbitrary) heating scale length. By comparing our simulated X-ray luminosities with those derived from ROSAT data (Table 2), our preliminary

**TABLE 1.** Stellar parameters for V374 Peg and AB Dor.

Star	Mass ( $M_{\odot}$ )	Radius ( $R_{\odot}$ )	$P_{rot}$ (d)	d (pc)
AB Dor	1.0	1.0	0.51	14.94
V374 Peg	0.3	0.35	0.45	8.963

**TABLE 2.** Simulated/observed X-ray properties for V374 Peg and AB Dor.

Star	$T_{corona}$ [iso] (MK)	log EM [iso] ( $\text{cm}^{-3}$ )	log EM [non-iso] ( $\text{cm}^{-3}$ )	log $L_X$ [iso] ( $\text{erg s}^{-1}$ )	log $L_X$ [non-iso] ( $\text{erg s}^{-1}$ )	log $L_X$ [obs, ROSAT] ( $\text{erg s}^{-1}$ )
AB Dor	10	52.48	52.75	29.69	29.94	30.18
V374 Peg	20	52.13	52.71	29.16	29.91	28.88

results suggest that such a non-isothermal coronal model works reasonably well for AB Dor with its complex magnetic structure, but fails for the simple field of V374 Peg.

## FUTURE WORK

We are currently adopting the models discussed by [9] and [10], in order to incorporate proper temperature profiles along coronal loops (Gregory et al, in preparation). Emission measure distributions (EMDs) will be derived and compared to those obtained from the observed X-ray spectra, allowing the validity of temperature scaling laws to be examined when used in conjunction with extrapolated magnetic fields. For such field structures, the loop geometry often departs from the semi-circular shape assumed by many previous studies (e.g. [8]). We will determine whether or not the same temperature scaling laws can be applied to both stars with complex magnetic fields (like AB Dor) and those with simple large-scale axisymmetric fields (like V374 Peg).

## REFERENCES

1. J.-F. Donati, and A. Collier Cameron, *MNRAS* **291**, 1–19 (1997).
2. J.-F. Donati, T. Forveille, A. C. Cameron, J. R. Barnes, X. Delfosse, M. M. Jardine, and J. A. Valenti, *Science* **311**, 633–635 (2006).
3. M. Jardine, A. Collier Cameron, and J.-F. Donati, *MNRAS* **333**, 339–346 (2002).
4. S. G. Gregory, M. Jardine, I. Simpson, and J.-F. Donati, *MNRAS* **371**, 999–1013 (2006a).
5. J. Morin, J.-F. Donati, T. Forveille, X. Delfosse, W. Dobler, P. Petit, M. M. Jardine, A. C. Cameron, L. Albert, N. Manset, B. Dintrans, G. Chabrier, and J. A. Valenti, *MNRAS* **384**, 77–86 (2008).
6. S. V. Jeffers, J.-F. Donati, and A. Collier Cameron, *MNRAS* **375**, 567–583 (2007).
7. S. G. Gregory, M. Jardine, A. C. Cameron, and J.-F. Donati, *MNRAS* **373**, 827–835 (2006b).
8. S. Serio, G. Peres, G. S. Vaiana, L. Golub, and R. Rosner *ApJ* **243**, 288–300 (1981).
9. A. Collier Cameron, *MNRAS* **233**, 235–256 (1988).
10. Y. C. Unruh, and M. Jardine, *A&A* **321**, 177–188 (1997).